Journal of Membrane Science 709 (2024) 123102

Contents lists available at ScienceDirect

Journal of Membrane Science

journal homepage: www.elsevier.com/locate/memsci

Ionic liquid mediated one-step perpendicular assembly in block copolymer thin films for ultrafiltration membrane applications

Kshitij Sharma [a], Khadar Basha Shaik [a], Maninderjeet Singh [a,1], Tanguy Terlier [b], Aidan Coffey [c], Chenhui Zhu [c], Joseph Strzalka [d], Alamgir Karim [a,*]

[a] William A. Brookshire, Department of Chemical & Biomolecular Engineering, University of Houston, Houston, TX, 77204, USA
[b] Shared Equipment Authority, Rice University, Houston, TX, 77005, USA
[c] Advanced Light Source, Lawrence Berkeley National Laboratory, Berkeley, CA, 94720, USA
[d] X-Ray Science Division, Argonne National Laboratory, Lemont, IL, 60439, USA

A B S T R A C T

The rapid rise of oil and gas, petrochemical, food processing, and pharmaceutical industries has added a complex mixture of contaminants like oil, particulates, metals, and other organic compounds to wastewater. Multipurpose membranes with precise pore structure can offer a solution to this problem and block copolymers (BCP) can be used to achieve such structures. Achieving vertical assembly of BCP domains provides a perfect template for developing uniform through film channels for separation and transport of material, besides being useful for the rectification of defects in photolithography patterns. Producing such morphologies may require extensive film/substrate processing and is not always feasible for scale-up. With this article, we demonstrate a facile solution casting method to induce vertical domain assembly in as-cast diblock copolymer thin films in the presence of an ionic liquid (IL) additive that preferentially segregates to one block and neutralizes interfacial interactions. We also show the tunability of domain sizes by controlling the additive concentration. These vertically aligned morphologies are important for the development of next-generation lithographic techniques and form excellent templates for ultrafiltration membranes with uniform pore sizes. This article demonstrates how IL additives can be used to obtain stable non-equilibrium morphologies in as-cast BCP films and the effect of BCP molecular mass, block volume fractions, and IL content on self-assembly.

1. Introduction

Facile self-assembly of block copolymers enables their application in nanolithography and tunable ultrafiltration membranes [1–12]. These applications require precise control of the domain sizes (L_o), the orientation of microdomains, and the grain sizes of the similarly aligned domains, i.e., the long-range order fidelity. Directed self-assembly techniques are mainly based on modifying or neutralizing the interfacial interactions between the polymer and the substrate while guiding the microstructure along a chemical pattern embedded in the substrate. This may also involve external fields that determine polymer chain alignment and, in turn, the domain orientation. In the presence of a block selective surface, the migration of polymer chains of that block to this surface directs the orientation of the BCP domains relative to the substrate which propagates to the film surface on long-time annealing [13]. For most lithographic applications, the domains should be perpendicular to the film surface, and processing approaches that prevent preferential migration of one block to the substrate are required, for instance, substrate surface energy modification, electric and magnetic field alignment, cold zone annealing, and solvent annealing [14–21].

Most of the techniques that orient BCP thin film domains require multiple film treatment steps, special equipment to apply external fields, or direct chemical modification of the substrate. On the other hand, the direct immersion annealing (DIA) methodology, which involves immersing a BCP film into a solvent mixture composed of film swelling and non-swelling solvents, can be used for facile assembly [22–26]. The solvent mixture swells the polymer film with neutral good solvents (reduces T_g) without causing any dewetting and imparts enhanced diffusive motion to the chains for faster assembly. Masud et al. have shown that the DIA solvent mixture composition can be tuned to neutralize interfacial energies for a film containing an ionic liquid additive (3–12 mass%) to orient domains perpendicular to the film surface [27]. They used an ionic liquid that selectively segregates to the methyl methacrylate block of a poly(styrene-*b*-methyl methacrylate) (PS-*b*-PMMA) BCP, neutralizing its favorable interaction with the SiO_x substrate. DIA can provide a simple pathway for rapid assembly but is

* Corresponding author.
E-mail address: akarim3@central.uh.edu (A. Karim).
[1] Current address: Department of Chemical Engineering, Columbia University, New York City, NY 10027, USA

https://doi.org/10.1016/j.memsci.2024.123102
Received 15 April 2024; Received in revised form 7 July 2024; Accepted 16 July 2024
Available online 17 July 2024

still an extra processing step after film fabrication. Simplifying further, solvent evaporation annealing (SEA) is a solvent processing technique that allows the microstructure to develop while the solvent(s) evaporates after casting. Two aspects need to be considered, the solvent evaporation rate and the solvent mixture quality (e.g. relative solubility) relative to the various blocks of the BCP and the substrate surface. These aspects effectively control the degree of order, the orientation of domains, and the in-plane order of the as-cast films.

Solvent cast morphologies have been studied before, for instance, the morphological study by Kim et al. for poly(styrene-*b*-butadiene-*b*-styrene) triblock copolymers where they found solvent evaporation rates can affect as-cast microstructures [28]. These methods have been developed to directly produce vertical morphologies such as that optimized by Seung et al., where they obtained vertical cylinders for a poly (styrene-*b*-ethylene oxide) (PS-*b*-PEO) diblock copolymer film spin cast from slow evaporating benzene solvent [29]. Ho et al. studied the formation of perpendicular hexagonal cylindrical morphology in poly (styrene-*b*-poly lactic acid) (PS-*b*-PLA) films by solvent evaporation [30]. They attributed the vertical orientation to the fastest solvent evaporation path available that depends on the strength of segregation between blocks and controls the kinetics of morphology development. Park et al. showed a similar technique for a high χ (Flory Huggins interaction parameter) poly(styrene-*b*-4-vinyl pyridine) (PS-*b*-P4VP) diblock copolymer cast from a solvent mixture of toluene and tetrahydrofuran (THF) showing morphologies ranging from micelles to vertical P4VP cylinders as the concentration of PS selective toluene decreases in the casting solvent mixture [31]. The combination of selective solvent interaction and controlled evaporation rates induces a microdomain transition from as-cast micelles to vertical cylinders.

Herein, we demonstrate that SEA in selective solvents traps a vertical morphology by enhancing the degree of segregation between blocks (enhanced χ) and eliminating preferential substrate-block interactions while swollen. While the addition of slow-evaporating neutral solvents to the casting solution may improve the degree of order due to more time for ordering, screened repulsion between blocks and the enthalpic influence of the substrate can significantly impact the morphology orientation. The χ parameter can be enhanced by doping with additives that selectively interact with a single block of the BCP and choose to segregate to that domain. Ionic liquids (ILs) allow for this approach. In addition to enhancing χ, ILs plasticize the BCP reducing its glass transition temperature, producing order in the rapid casting step. Bennet et al. studied symmetric diblock PS-b-PMMA BCPs with 1-ethyl-3-methylimidazolium bis(trifluoromethanesulfonyl)amide (EMIM-NTf_2) IL additive [32]. They observed enhanced order in ultrathin films (thickness, h $\approx L_o$) of difficult-to-order very low molecular mass BCPs after high temperature thermal annealing in nitrogen due to enhancement in χ (IL is PMMA selective) at IL contents of 5 mass% relative to the BCP. They further showed that the addition of more IL increased the domain size by up to 10 nm at an IL concentration of 12 mass%. At a higher concentration of 17 mass%, the morphology transitioned to hexagonally packed cylinders due to a large deviation in the volume fractions of the blocks owing to the selective swelling by the IL. Chen et al. studied different ILs to enhance χ for low molecular mass PS-b-PMMA to achieve sub-10 nm domains and observed the same trend of increasing domain sizes with IL content for vertical assembly on substrate grafted with a random copolymer brush [33]. Masud et al. used a 1-ethyl-3-methylimidazolium bis(trifluoromethylsulfonyl)imide (EMIM-TFSI) IL with high molecular mass PS-b-PMMA to show enhanced parallel lamellar assembly with low defect density for thermally annealed films with large thicknesses [34].

In addition to inducing vertical assembly using much simpler SEA compared to the conventional TA or SVA on a random copolymer brush, we hypothesized that the amount of IL in the BCP film can be tuned to directly get vertical order in as-cast films on unmodified substrates and simultaneously control domain size. Fig. 1 describes the SEA-IL approach of one-step ordering along with the proposed ordering mechanism which we will discuss later. This is based on a competition between favorable interactions of PMMA/IL and PMMA/SiOx vs repulsive interactions between IL/SiOx and IL/PS. Figs. S1 and S2 in the supporting information show contact angle measurements for the EMIM-TFSI and dewetting of an IL film on UVO-treated Si substrate (SiO_x), respectively. These measurements support the hypothesis of attractive interaction between PMMA and IL and repulsive interactions between SiO_x and IL.

With this research, we demonstrate a SEA-IL methodology to order and orient BCP domains in as-cast low χ and low molecular mass PS-b-PMMA thin films. The technique involves casting thin films from a solvent formulation composed of neutral, partially selective, and selective solvents that plasticize the system, enhance the BCP interaction parameter (χ), and neutralize interactions at the substrate and air interface to impart vertical morphology in the as-cast state. Contrary to most previous observations, we show that cylindrical (*cyl*) BCP films can be loaded with much larger quantities of IL (up to 150 mass% with respect to the BCP film mass) before a morphological change or macrophase separation occurs. These concentrations are even higher than the amount that PMMA homopolymer thin films with molecular masses close to the mass of PMMA block in the BCP can hold (up to 30 mass% relative to the homopolymer PMMA film mass) without macrophase separation. AFM phase images for homopolymer PMMA (M_n = 15 k) films are shown in Fig. S3. The presence of the structural PS block in the BCP that does not interact with the IL may have a significant role in supporting a stable film and conserving the cylindrical morphology at very high IL contents. With the right choice of solvents and ionic liquid, this casting formulation can be translated to other block copolymers to obtain vertical microstructures for nanolithography, advanced ultrafiltration membranes, polymer electrolytes, etc.

2. Materials & methods

2.1. Experimental design

Thin films of a diblock copolymer were cast on silicon substrates using the ionic liquid based solvent evaporation annealing (SEA-IL) method. The processing conditions (time, temperature, solvent mixtures, etc.) were chosen to explore the BCP self-assembly and morphology evolution in as-cast films.

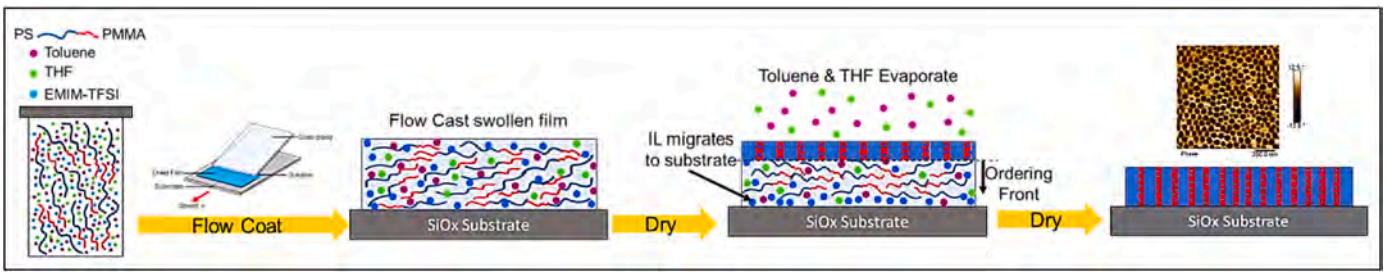

Fig. 1. One-step ordering mechanism for through film vertical domain assembly in ionic liquid-filled thin block copolymer films by flow coating.

2.2. Materials

Polystyrene-*b*-Poly(methyl methacrylate) (PS-*b*-PMMA) diblock copolymers were acquired from Polymer Source Inc. with number average molecular mass of M_n = (55 k-b-22 k), (35 k-b-12.5 k), (33 k-b-33 k), and (235 k-b-263 k) g/mole. Poly(styrene-*b*-4-vinyl pyridine) (PS-*b*-P4VP) with M_n = (67 k-b-27 k) g/mole and Poly(styrene-*b*-ethylene oxide) (PS-*b*-PEO) with M_n = (68 k-b-36 k) g/mole were also obtained from Polymer Source Inc. Poly(methyl methacrylate) (PMMA) with M_n = 15 k g/mole was obtained from Sigma Aldrich. All block volume fractions correspond to an asymmetric diblock except for the diblock with M_n = (33 k-b-33 k) and (235 k-b-263 k) g/mole which have a symmetric volume fraction. BCP solutions were made in mixtures of laboratory-grade toluene (VWR BDH Chemicals, ACS reagent, ≥99.5 %), Tetrahydrofuran (THF – Macron Fine Chemicals (stabilized), ACS reagent) and Acetone (VWR BDH Chemicals, ACS reagent, ≥99.5 %) with a 3 mass% to 5 mass% concentration. Acetic acid (glacial) is a ACS grade reagent and was obtained from Sigma Aldrich. The ionic liquid 1-Ethyl-3-methylimidazolium Bis(trifluoromethanesulfonyl)imide (EMIM-TFSI) was obtained from TCI Chemicals with purity >98.0 %.

2.3. SEA-IL methodology for BCP films

Thin films were cast from solutions of PS-b-PMMA of different molecular masses and volume fractions using the flow coating method. The polymer solution concentration was ≈40 mg/ml plus the mass of IL at various concentrations relative to the polymer mass. Flow coating requires only minute quantities of the polymer solution. The polymer solution was pipetted into the gap between an angled glass blade and a flat *Si* substrate (substrate is Ultraviolet Ozone (UVO) treated for 120 min). The blade edge moved along the substrate, pulling the bulk of the solution along with it and coating a thin layer onto the substrate. Films were also prepared using a standard spin coating method to confirm the effects of the film coating technique on the SEA morphology.

2.4. Membrane fabrication

Films ≈100 nm thick were cast onto a thin layer of water soluble PSS (poly(4-styrene sulfonic acid)) precoated on Si substrates. The films were floated off on the surface of water in a bath. These free-floating films were captured on commercial PES (poly ether sulfone) support membranes. The films on PES were treated under UV-light in vacuum to crosslink PS and etch PMMA. The illumination durations ranged from 10 min to 60 min. The UV light wavelength and intensity are 254 nm and ≈4.84 mW/cm^2. The membranes with crosslinked/etched BCP topcoat were immersed in glacial acetic acid bath for 10 min to dissolve away the etched PMMA and the IL. The rinsed membranes were dried overnight at room temperature before performance measurements. Drying was also done in vacuum (≈100 kPa) at 60 °C to check for variability with the air-drying method and no differences were observed.

2.5. Characterization Methods

Film thicknesses were measured using UV–vis interferometry on the Filmetrics LS-DT2 interferometer. The topography of the polymer-air interface for thin films was characterized using atomic force microscopy (AFM) on the Bruker AXS Dimension Icon in standard tapping mode in air. Height sensor and phase scans were obtained for all film samples. The images were flattened using Bruker Nanoscope Analysis software by the first order to fit each line individually and remove tilt. Scanning Electron Microscopy (SEM) imaging was done at the University of Houston Nanofabrication facility using the FEI Dual Beam 235 Focused Ion Beam instrument. Some SEM measurements were also performed at Columbia University, NY. The SEM image contrast was enhanced using ImageJ software. Grazing incidence small angle x-ray scattering was performed on solid films at the Advanced Light Source, Lawrance Berkeley National Lab on beamline 7.3.3 and at the Advanced Photon Source, Argonne National Lab on beamline 8-ID-E. The results presented are for grazing incidence angle of 0.16° which is above the critical angles for PS, PMMA, and Si. Optical microscopy was done using an Olympus microscope (BX-41) in reflection mode. Time of Flight Secondary Ion Mass Spectroscopy was performed using the ION TOF ToF-SIMS NCS instrument at RICE University's shared equipment authority. UV-visible spectroscopy measurements were performed on the Evolution 201 UV–Visible Spectrophotometer from ThermoFisher scientific and zeta potentials were measured on the Anton Paar SurPASS 3.

3. Results & discussion

Directing self-assembly of BCP domains perpendicular to the substrate is highly desirable but often not trivial and may require complex instrumentation and multiple processing steps to obtain highly ordered microstructures. The fidelity of the order both in and out of the plane of the film is essential to their application in nanolithography. Some of the solution casting methods introduced previously produce vertical microstructure right after the casting step but are limited to relatively higher χ BCPs. Here we demonstrate a solution casting method that produces perpendicular microstructure in as-cast films and allows for size tunability by modifying the casting solution formulation. We use a low χ PS-b-PMMA BCP with both symmetric (*sym*) and asymmetric (*asym*) block volume fractions and with variable molecular masses (M_n) to study the SEA process. The polymers used and their theoretical morphologies based on relative block volume fractions are listed in Table 1.

Asym PS-b-PMMA with M_n = 55 k and 22 k (g/mol) for PS and PMMA blocks, respectively, has a hexagonal cylindrical (HC) morphology with PMMA forming the cylindrical domains. Films were cast using the flow coating method from pure toluene and a solvent mixture of toluene and tetrahydrofuran (THF) on UVO (Ultraviolet ozone cleaning) treated silicon wafers. The UV ozone treatment burns off any organic residue and oxidizes the substrate to form a thin SiO_x layer. PMMA being preferential to this oxide layer segregates to the substrate and induces a parallel HC morphology upon annealing thermally or in a solvent mixture or solvent vapor environment [27]. To prevent this selective migration, the interfacial forces need to be neutralized. While grafting a random copolymer brush is an established method to neutralize the substrate, it is an extra step in the processing strategy. To circumvent it, we speculate using the unfavorable interaction of IL with SiO_x and favorable interactions with PMMA (Figs. S1 and S2) and hypothesize that for a certain IL concentration window in the casting solvent mixture, the preferential substrate interactions can be neutralized. At and beyond this lower end of the IL concentration window, we term as the critical IL composition (IL_c) for "neutralization" of PMMA wettability to SiOx, PMMA swelling-induced osmotic pressure drives a partitioning of the IL to the substrate. Regarding how thin of an IL layer that partitions to the substrate and neutralizes PMMA wetting to the SiO_x will be the subject of future research, measured using X-ray and neutron reflectometry, as ToF-SIMS is unable to determine this accurately in the current paper. Beyond the critical concentration required to induce vertical assembly, PMMA cylinders can continue to swell more as even

Table 1
Diblock copolymers studied in this work, their molecular masses, and theoretical morphologies.

Block Copolymer	Molecular Mass (kg/mol)	Morphology (Based on block volume fractions)
PS-b-PMMA	35-b-12.5	Cylindrical
PS-b-PMMA	33-b-33	Lamellar
PS-b-PMMA	55-b-22	Cylindrical
PS-b-PMMA	235-b-263	Lamellar
PS-b-P4VP	67-b-27	Cylindrical
PS-b-PEO	68-b-36	Cylindrical

higher quantities of IL are added.

3.1. Atomic force microscopy analysis of SEA-IL cast film morphology

We test the above hypothesis by casting films from solvent mixtures with variable IL content relative to the BCP mass (all IL contents are relative to the film mass). Fig. 2 shows the AFM phase images for PS-b-PMMA (55 k-b-22 k) films cast at room temperature with a thickness of ≈100 nm and variable IL concentration from a 50/50 (v/v) solvent mixture of toluene and THF, with 2D-Fast Fourier Transform (2D-FFT) spectra shown in the inset. The images in Fig. 2 have a darker color for softer phases/domains and can be seen as the darker background of the softer PS (Lower T_g) matrix in the AFM phase image for BCP with no IL in Fig. 2(a). The contrast variation in phase images have been previously reported and show a similar trend as seen here [35–37]. The film surface shows nucleated cylindrical domains in a light color for the stiffer PMMA (Higher T_g) domains. The segregation strength for the system is very low as the films were cast from a solvent mixture of toluene and THF, good solvents for both blocks. With the addition of 5 mass% IL in the solvent mixture, the films show (Fig. 2(b)) limited assembly with a majority of cylinders packed parallel to the surface (seen as dark worm-like lines in the AFM image) and a minority of vertical cylinders still seen in a lighter color. The parallel cylinders have a darker color due to the presence of PS chains surrounding PMMA cylinders. The vertical cylinders on the other hand directly show the stiffer PMMA domains. At 20 mass% IL content, the reduction in T_g is significant and the preferential segregation of the IL to the PMMA domain increases the effective χ ($\chi_{eff} > \chi_{BCP}$) improving the overall assembly manifolds. However, the microstructure still has long parallel cylindrical domains on the film surface indicating that the substrate neutralization is not strong enough even at 20 mass% IL. We see a change in color for the cylindrical domains here (parallel and vertical) as the IL content is also high enough to lower the T_g for PMMA below that of PS. We know that the cylinders are still made of PMMA from the results of a selective etching experiment described later in the paper. When the IL content is increased to approximately 25 mass%, completely vertical PMMA cylinders develop on the surface of the film (Fig. S4 shows AFM morphology for 23 mass% and 27 mass% IL films). Previous studies report a transition in morphology due to large volume fraction changes [32,38] which was not observed here for the SEA-IL method. At the threshold of 30 mass% IL, the microstructure transitions to IL-filled cylinders (in a darker color) aligned completely perpendicularly/vertically relative to the film surface. This implies that at this IL content, the BCP system achieves synergy between ordering and domain orienting interactions, i.e., in addition to enhancing the ordering strength by segregating to the PMMA domain enabling self-assembly in a single casting step, the migration of IL to the substrate screens preferential wetting between the PMMA block and the substrate and thus induces vertical orientation as hypothesized. Thus, solvent evaporation annealing with ionic liquid (SEA-IL) can yield perpendicular microstructure in a single casting step.

The cylinder diameters are highly swollen compared to the natural domain size of the BCP (compare Fig. 2(b) vs. 2(f)). The 2D-FFT plots in the inset show both secondary and tertiary rings at 30 mass% IL content indicating the best in-plane order among the compositions tested. The HC arrangement can also be easily inferred from a visual inspection of the AFM phase images. With further increase in the IL contents (40, 50, and 60 mass%) the swelling of the PMMA cylinders increases and the in-plane cylinder arrangement starts losing the hexagonal symmetry. In comparison, homopolymer PMMA films are unable to hold such high quantities of ionic liquid and we observed macrophase separation using AFM as well as optical microscopy at 30 mass% IL (AFM and Optical microscopy images in Fig. S3 show macroscopic phase separation in IL-filled PMMA thin films). The tunability of BCP domains have been previously shown by using acetic acid to swell the PMMA domains of a PS-b-PMMA diblock [6]. Tuning the pore structure of the BCP membranes have also been shown by using various casting methods and studied for targeted filtration applications [39–42].

In comparison to the homopolymer, even at 70 mass% IL content, BCP films only show microphase separation into highly swollen cylinders with signs of laterally elongated domains likely produced by two cylindrical domains merging. We also observe deviation in the circularity of the vertical cylinders due to extensive swelling. The domain coalescence is more pronounced with an IL concentration of 100 mass%. The swollen and merged cylindrical domains are present up to an IL concentration of 150 mass% beyond which macroscopic IL-filled domains become visible. Fig. S5 of the supplementary information shows phase images for the 150 mass%, 175 mass%, and 200 mass% IL-BCP films. For the 175 mass% and 200 mass% IL-BCP films,

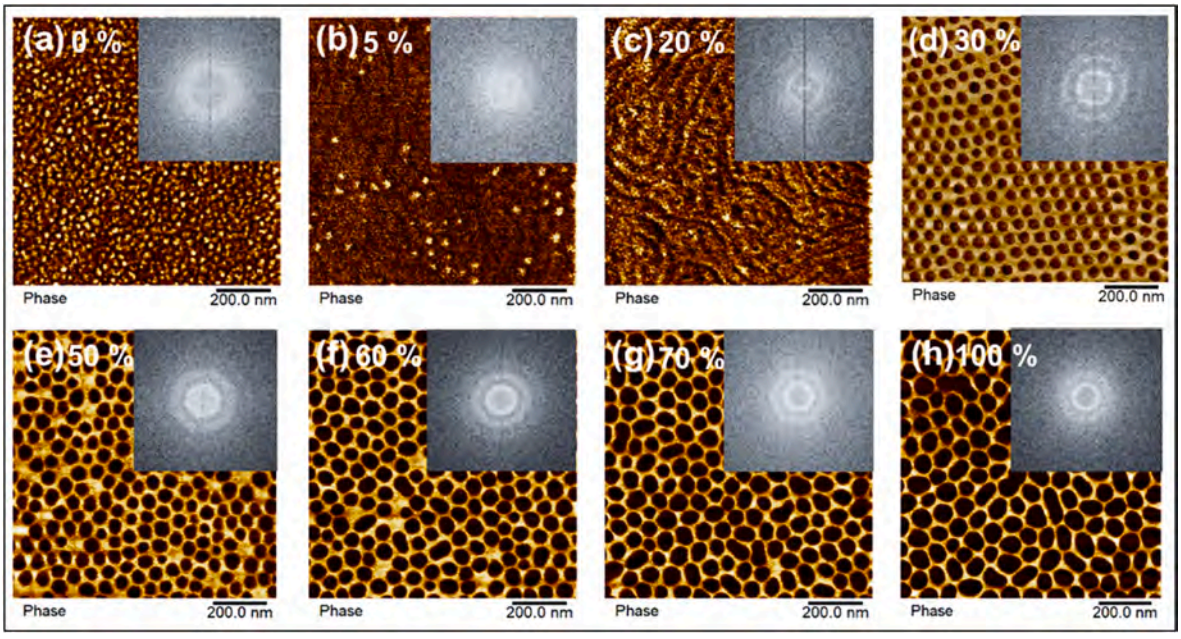

Fig. 2. AFM phase images and 2D-FFTs for as-cast PS-b-PMMA (55 k-b-22 k) films ≈ 100 nm thick on SiO_x substrates with IL contents in mass% relative to the BCP film of a) 0 %; b) 5 %; c) 20 %; d) 30 %; e) 50 %; f) 60 %; g) 70 %, h) 100 %.

macroscopically segregated domains can be seen in the AFM phase image. The microstructure parameters like average lengths of cylinder diameter and inter-cylinder distance along with the cylinder/pore density were calculated at various IL contents using ImageJ analysis on AFM phase images and are plotted in Fig. 3. These average lengths increase with the increase in IL content. While the film surface shows excellent vertical cylindrical assembly, information on internal film structure cannot be derived from AFM surface scans only. We therefore employed, as a first, a simple method to look for the cylinder orientation at the film-substrate interface. Poly(styrene sulfonic acid) (PSS) is a water-soluble polymer. The sulfonated nature of PSS makes it preferential to the more polar PMMA block very similar to SiO_x.

A thin PSS film (20 nm–30 nm) can be used as an underlayer on the SiO_x substrate before casting the BCP film on top. This provided us with a way to float off the BCP films onto the surface of water, flip them over, and look at the film-substrate interface with an AFM. The scans are shown in Fig. 4 with height sensor images of the top and bottom of the film (presentable phase images could not be obtained for the water-floated films). Both surfaces show the vertical assembly of PMMA cylinders. This result suggests that the IL can screen interactions with a variety of surfaces and the combined effects of IL plasticization, IL selectivity (enhanced χ), and rapid solvent evaporation traps the entropically favorable perpendicular orientation. These PMMA domains can be etched using a simple UV illumination in vacuum treatment to crosslink PS and etch PMMA followed by a glacial acetic acid rinse to wash away the etched PMMA [43,44]. Processing the films this way etches out the cylinders that confirm the presence of PMMA only in the cylindrical domains and the creation of deep pores indicates a through-film vertical cylindrical assembly. Fig. 4(c) shows an AFM height sensor image of an etched film having circular pores on the surface in place of the IL-swollen PMMA cylinders. The pore depths are not fully resolved due to limitations with the AFM tip having μm dimensions. AFM measurements were also done for etched films on a softer PES supports and are shown in Fig. 4(d). The flexibility of the support membrane distorts the pore structures when measured by AFM and may be better resolved using SEM. The ionic liquid, EMIM-TFSI, used here is miscible with acetic acid and dissolves in acetic acid along with the PMMA giving clean and structured pores. This was

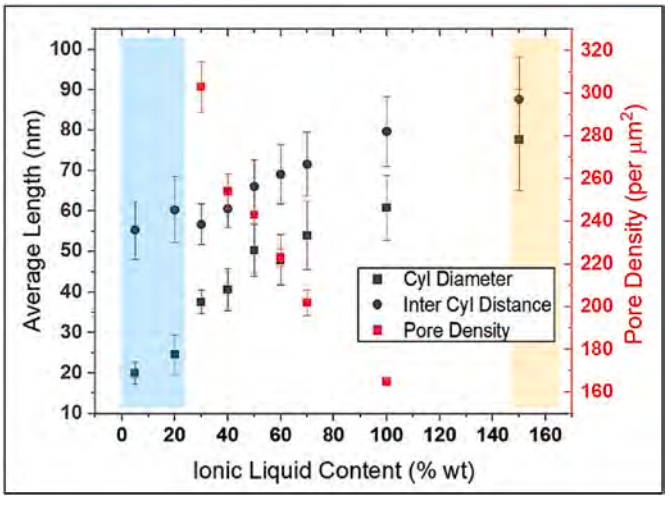

Fig. 3. Average lengths for the cylindrical PMMA domains on the film surface for as-cast PS-b-PMMA (55k-b-22k) films (≈100 nm thick) with varying ionic liquid content (relative to film mass). The error bars are one standard deviation. The shaded light blue region from (5–25) mass% IL corresponds to poorly developed surface parallel cylinders, above which are vertical IL swollen PMMA cylinders. The shaded yellow region is where macrophase separation is observed. (For interpretation of the references to color in this figure legend, the reader is referred to the Web version of this article.)

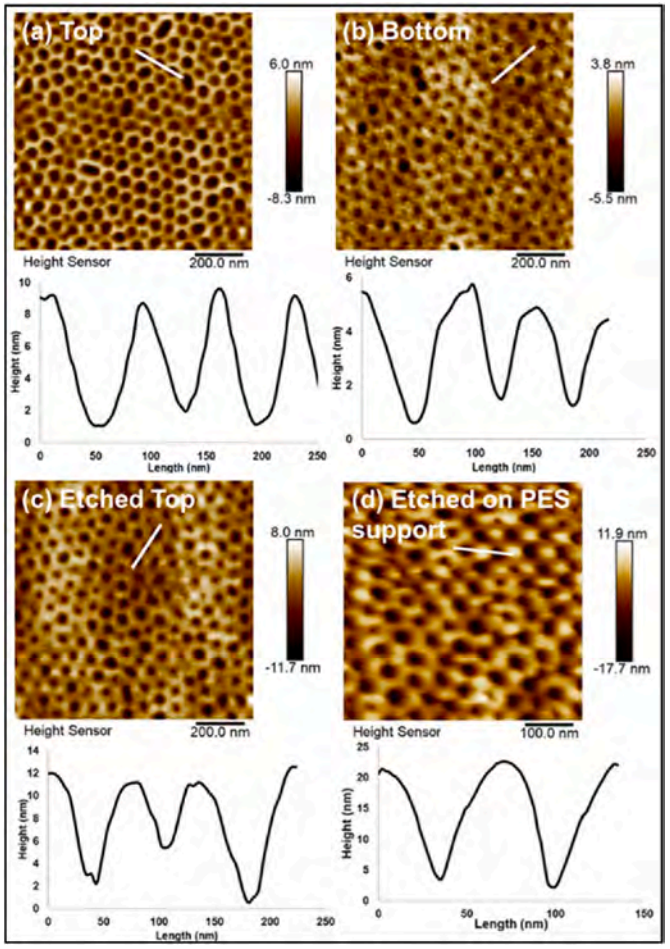

Fig. 4. AFM height sensor images for the (a) top and (b) bottom surfaces of an as-cast PS-b-PMMA (55 k-22 k) film 100 nm thick with 50 mass% IL content on Si substrate, and (c) after etching by UV-vacuum treatment (10 min) and acetic acid immersion (30 s), (d) film on 0.2 μm PES support after etching via UV-vacuum (10 min) and acetic acid treatment (10 min). Height profiles along marked white lines in the AFM images are presented below each image.

confirmed with ToF-SIMS experiments, where the IL and PMMA signal intensities drop by an order of magnitude for etched films compared to the as-cast ones (Fig. S6). The IL signal is intensified due to the higher sensitivity of the detector towards it, but we see an order of magnitude decrease in its intensity after etching. The ToF-SIMS experiments were performed for films on SiO_x substrates leading to residual IL near the substrate after etching. We expect that in a membrane module with soft, porous support, the IL and scissored PMMA chains will be completely removed on acetic acid rinsing.

In addition to AFM measurements, we have employed side view SEM imaging to confirm the pore structure. Fig. 5(a) shows the top surface of an etched film folded onto the edge of the snapped Si wafer showing well-ordered pores on the top. Fig. 5(b) shows the side view of the edge of an etched films showing open pores. The direct snapping method damages the film edge preventing us from displaying the exact microstructure. Unetched films don't have very high contrast between the domains. We can, however, observe pore/cylinder wall boundaries as perpendicular lines underneath the pores corresponding to the pore walls in Fig. 5(c). These lines or pore walls have been marked in Fig. 5(d) for visual clarity.

3.2. *X-ray scattering characterization of internal film morphology*

To corroborate our assumption of through film vertical assembly

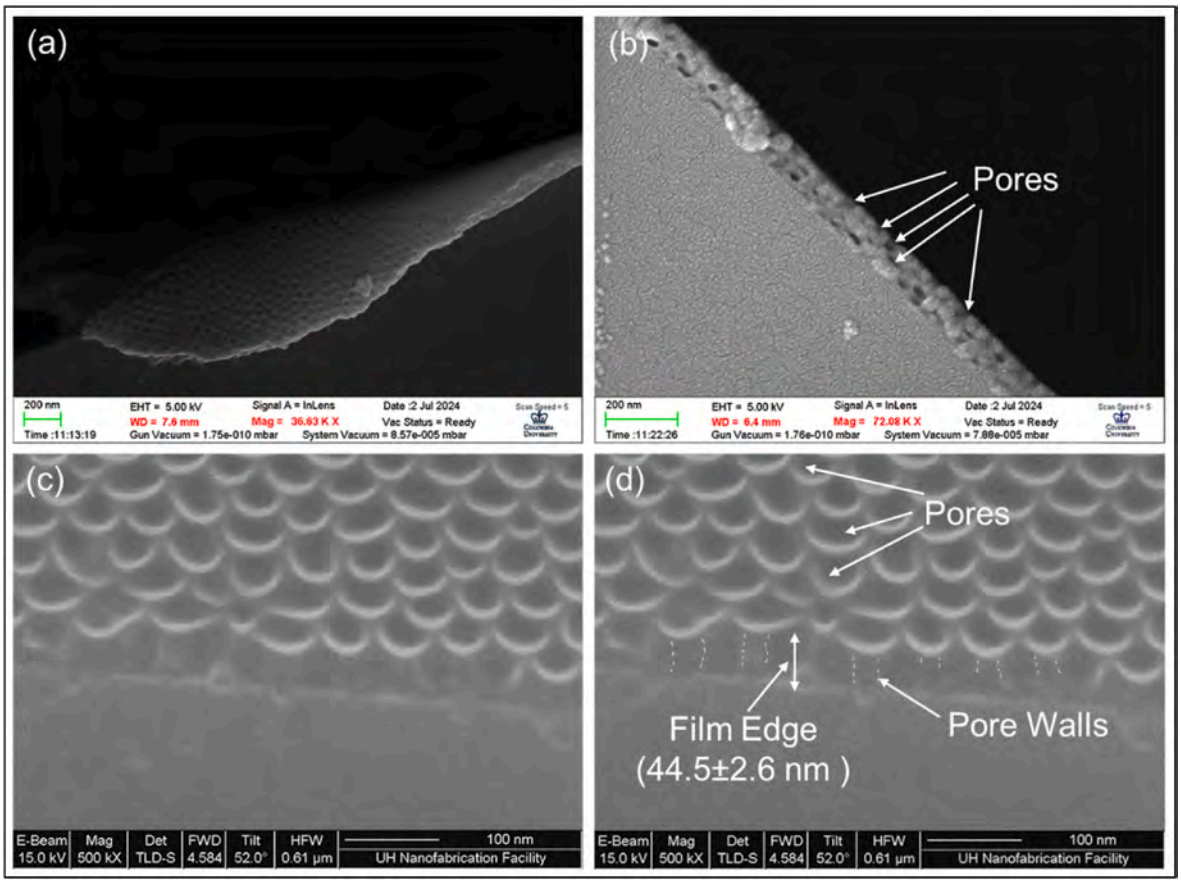

Fig. 5. Side view scanning electron microscopy images for PS-b-PMMA films (thickness ≈ 100 nm (a, b) and 50 nm (c, d)) with 50 mass% IL cast on Si substrates. (a) top view of etched film, (b) side-view of the etched cross-section, (c) side-view of unetched film cross-section, (d) side-view of cross-section in (c) with marks for feature identification. The error in thickness measurement is one standard deviation.

made using AFM, grazing incidence small angle x-ray scattering (GISAXS) experiments were performed on a series of PS-b-PMMA (55 k-b-22 k) films with varying IL contents and two thicknesses. The collected data for the entire series is presented in Figs. S7 and S8 of the supplementary information. From these scattering images, two sets are shown in Fig. 6 for IL contents of 50 mass% and 70 mass% and thicknesses of ≈50 nm and ≈100 nm. For a fully vertical structure, the peaks in the scattered intensity should only be along the Q_y axis, while there is an isotropic ring for scattering from a mixed parallel and vertical microstructure. For the 50 mass% IL film the isotropic ring disappears as the film thickness decreases from 100 nm to 50 nm. Similarly for the 70 mass% IL film vertical assembly becomes dominant on decreasing the film thickness.

Such film thickness dependence on morphology has been studied before and shows a transition between perpendicular, mixed, and parallel orientation with changes in thickness [45,46]. While film thicknesses less than the domain size ($h < L_o$) develop perpendicular orientation, thicker films transition between morphologies as a function of thickness. Our observations on morphology orientation with film thickness after thermal annealing of the pure PS-b-PMMA (55 k-b-22 k) ($T_g \approx 120$ °C) films (No IL) of two thicknesses annealed thermally at 180 °C for 24 h in vacuum are shown in Fig. S9. While the thicker film

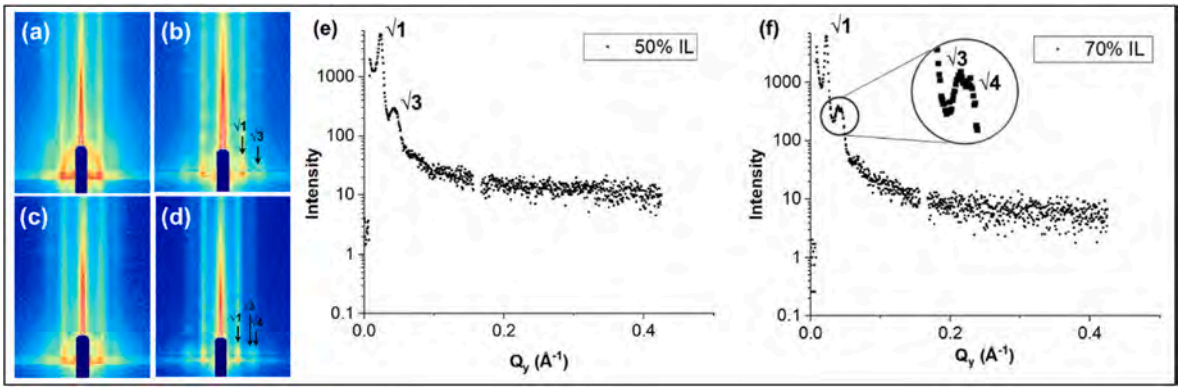

Fig. 6. GISAXS scattering pattern (above critical angle) for as-cast PS-b-PMMA (55 k-b-22 k) thin films with variable IL content and thickness of a) 50 mass% and 100 nm; b) 50 mass% and 50 nm; c) 70 mass% and 100 nm; d) 70 mass% and 50 nm, (e) intensity line curves from scattering image of 50 nm film with 50 mass% IL, (f) intensity line curves from scattering image of 50 nm film with 70 mass% IL.

(Fig. S9(b)) has more vertical cylinders on the top surface to reduce surface curvature/roughness, the thinner film (Fig. S9(c)) has more parallel cylinders indicating a stronger influence of the substrate's PMMA attraction when annealed thermally. In our study using SEA, a lower film thickness provides better vertical order which is due to faster solidification of the film on solvent evaporation preventing any significant influence of the substrate or air interfaces. Comparing Fig. 6b and d, i.e., different IL concentrations, the intensity of the scattered peaks increases, the isotropic ring disappears, and secondary peaks are observed at 70 mass% IL compared to 50 mass%, indicating enhanced assembly. The scattered intensity can be plotted along the Q_y axis to assign positions to the peaks. Fig. 6(e) and (f) show these plots for images 6(b) and 6(d) where the relative positions of the peaks have a ratio very close to the hexagonal symmetry of $\sqrt{1}:\sqrt{3}:\sqrt{4}$. The scattering data thus corroborates the inference of a vertical HC assembly observed for the AFM study and shows enhanced vertical ordering at lower film thickness and higher IL concentrations.

3.3. Effects of molecular mass and block volume fractions on morphology and transitions

This SEA-IL methodology was used to self-assemble a low molecular mass asymmetric PS-b-PMMA (M_n = 35 k-b-12.5 k g/mol). The as-cast films show good vertical cylindrical assembly in a certain range of IL concentrations. Fig. S10 shows AFM phase images and GISAXS wave plots for these thin films with different IL concentrations. Phase images for neat BCP films do not show any microphase separation on the surface. At only 10 mass% IL content, some degree of vertical order is already present because of the higher chain mobility due to reduced T_g of the low M_n BCP [47], not requiring extensive plasticization from the IL. The PMMA domains are still stiffer than PS and appear in a lighter color. With further increase in IL content to 30 and 40 mass%, the vertical order improves and can be seen in the phase images now as darker cylinders because there is a significant reduction in the T_g of IL-filled PMMA domains. The same is observed in the GISAXS images in Fig. S10 insets where the scattering peaks corresponding to vertical structure become more intense as IL concentration increases. These lower M_n films however, exhibited an early deviation from vertical cylindrical assembly towards merged cylindrical domains over 40 mass% IL content (Fig. S10(d) for 50 mass% IL) and extensively elongated domains at 70 mass% IL content. Films with 100 mass% IL concentration show macrophase separation of the ionic liquid with no cylindrical assembly. These percentages for morphology transition are approximately half of what moderate molecular mass *cyl* BCP (M_n = 55 k-b-22 k) could hold before showing macrophase separation.

Symmetric block copolymers produce lamellar microstructures and are essential in developing techniques to obtain line patterns for applications in nanolithography, shape-selective filtration membranes, etc. To extend the SEA-IL annealing treatment further, we used a symmetric low molecular mass PS-b-PMMA with M_n = (33 k-b-33 k). As shown in Fig. 7, the morphology without IL is mostly disordered with some microdomain initiation at the film surface. On blending with just 10 mass% IL the films show excellent vertical lamellar assembly on casting from toluene and THF (50/50; v/v). GISAXS wave-plots presented in the inset show sharp scattering peaks confirming vertical morphology. The PMMA domain is swollen and appears thicker in the AFM image producing an asymmetric vertical lamellar microstructure with PS domain size ≈18 nm (measured using ImageJ analysis). Increasing the IL content to 30 mass% alters the volume fraction of the blocks significantly and the morphology reverses to form PS cylinders (stiff–light color) having a mixed parallel and perpendicular orientation in a PMMA (soft–dark color) matrix. When the IL content reaches 50 mass% macrophase separation becomes significant on the film surface and bigger macrodomains appear with the increase in the ionic liquid concentration to 70 mass% and 100 mass% (Fig. S11). The morphology evolution and orientation for low M_n *sym* BCP films follow the same trend as low M_n *asym* BCPs. The morphology switches from a surface-influenced parallel microstructure to a perpendicular microstructure at lower IL contents and we observe a significant deviation in block volume fractions at intermediate concentrations (20–30 mass%) of the additive leading to a morphology transition.

Very High M_n BCPs are difficult to process due to higher T_g and poor diffusion kinetics in the melt. Even solvent processing methods like SVA and DIA are limited by molecular masses as high as the one studied next for PS-b-PMMA with M_n = (235 k-b-263 k) g/mole. We use the SEA-IL casting technique to prepare thin films of this BCP with 50 mass% IL and perform AFM analysis presented in Fig. S12. We observe a well-ordered cylinder-like morphology for the symmetric BCP in as-cast films without needing further processing. This may be the first demonstration of self-assembly achieved in high molecular mass BCP thin films which is achieved in a single casting step. The cylindrical domains were removed using a method that etches out the PMMA domains leaving behind deep pores in the film suggesting PMMA and IL to be the constituents of the cylindrical domains. This is counterintuitive as one would expect PMMA + IL to have a higher volume fraction at high IL contents causing a transition in morphology to PS cylinders in a PMMA + IL matrix. The presence of PMMA + IL in the minor domains may be the result of the high cohesive energy density of the IL causing it to occupy domains with smaller surface area. A preliminary GISAXS study reveals sharp scattering peaks for this morphology at very low q-vector positions (inset of Fig. S12(b)). The microstructure needs further analysis with techniques like X-ray scattering and a complete study with varying IL concentrations for morphology development using the SEA-IL method.

SEA-IL is demonstrated here for a PS-b-PMMA BCP but can be formulated for other low and high χ diblock copolymers like poly(styrene-*b*-ethylene oxide) and poly(styrene-*b*-vinyl pyridine), respectively. The IL contents and solvent selections will vary based on the solubility of the BCP, the strength of its interaction with the selective IL and the substrate, and the type of interaction between the IL and substrate. Even

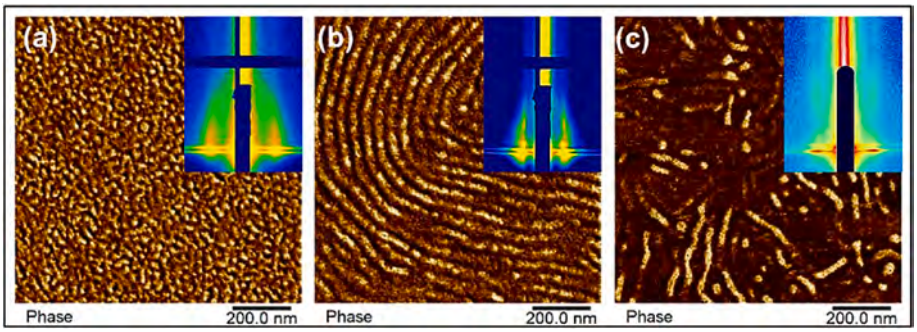

Fig. 7. AFM phase images for PS-b-PMMA (33 k-b-33 k) films (≈100 nm) cast from a solvent mixture of Toluene:THF (50:50; v/v) with (a) 0 mass% IL, (b) 10 mass% IL, (c) 30 mass% IL.

low molecular mass polymers may show promising results toward achieving directed self-assembly with features smaller than 20 nm. As an example, PS-b-P4VP (67 k-b-27 k) and PS-b-PEO (68 k-b-36 k) were ordered using the SEA-IL method using the same IL, EMIM TFSI. The films were cast from a solvent mixture of toluene and THF, where toluene is a good solvent for PS and a poor solvent for PVP and PEO, and THF is a good solvent for the IL, the PVP, and the PEO blocks. PS-b-PEO films were also cast from THF and toluene-acetone mixtures. The AFM analysis for PS-b-P4VP is presented in Fig. S13 Row 1. For PS-b-P4VP, a high χ BCP, the vertical orientation is achieved at 20 mass% IL concentration, and at 50 mass% IL, the films show domain merging and macrophase separation at even higher IL concentrations. Similarly for a low χ BCP like PS-b-PEO, films were cast with and without IL in solvent mixtures of toluene, THF, and acetone to extend our hypothesis and check morphology variations for films cast from different solvents. Fig. S13 Row 2 presents the AFM phase images for SEA-IL cast PS-b-PEO films. Films cast from toluene and THF (50/50 v/v) show some degree of vertical assembly of PEO cylinders even without IL and at 50 mass% IL concentration show well-developed IL swollen vertically oriented PEO cylinders. When cast from a solvent mixture of toluene and acetone where acetone is a poor solvent for PS unlike THF and a good solvent for the IL and PEO, films develop larger IL swollen cylindrical domains. This may be due to a higher segregation of IL along with acetone into the PEO domains while swollen with the solvent which gets trapped (only IL) on solvent evaporation. When cast from pure THF, the PS-b-PEO films show macrophase separation and no cylindrical assembly at 50 mass% IL concentration. Additionally, using different proportions of toluene and THF instead of the 50/50 (v/v) mixture can affect the in-plane arrangement of ordered domains as it will affect the evaporation rate (or ordering time). These tests suggest that the morphology of the SEA-IL cast films can be further tuned by modifying the proportion and quality of the volatile solvents.

3.4. Ionic liquid additive as interfacial neutralizing agent

The one-step perpendicular ordering of BCP films is a cumulative result of three major contributors, 1) plasticization by the IL; 2) enhancement in repulsive interaction (enhanced χ) due to the selective segregation of IL into one domain; and 3) screening of the preferential migration of blocks to the substrate or air interface due to interfacial energy differences, all of which can be adjusted for various BCP materials by carefully selecting the casting environment. To understand the role of IL in inducing vertical assembly better, ToF-SIMS depth profiling was performed on PS-b-PMMA films cast on SiO_x substrates and the results indicate that there is a higher quantity of IL present near the film-air interface as well as the film-substrate interface relative to the middle of the film. This confirms our hypothesis that the IL segregates not only to the PMMA domains but also to the interfaces in conjunction with PMMA and when the mass fraction of IL in the film region near the substrate is above a critical value (IL_c), a balance between the interfacial forces is established leading to screening of the enthalpic interactions and an entropically stable perpendicular morphology is produced. The schematic in Fig. 1 also describes this hypothesis. For instance, the IL_c for PS-b-PMMA with M_n = 55 k-b-22 k is at 25 mass% IL for the onset vertical assembly, and the following condition is satisfied at the substrate interface,

$$\chi_{PS-SiO_x} = \chi_{(PMMA+ILc)-SiO_x}.$$

Additionally, we hypotheisze that the macorscopic IL layer near the substrate decouples the BCP chains from the hard substrate interaction. This allows for high degree of mobility as the chain arrangement takes place on a fluid IL layer. Above IL_c content, the BCP remains vertical, but extra IL is imbibed by the PMMA, and a second weaker order threshold transition occurs, when the IL_{c2} forms its own pure IL liquid channel probably in the middle of the PMMA domain after swelling the domain to the fullest extent, e.g., AFM phase images in SI Figure S5(a) suggests $IL_{c2} \sim$ 150 mass% when the PMMA-IL cylinder diameter exceeds $\approx$ 75 nm. This will be studied in future works using techniques like resonant soft x-ray scattering (RSoXS). Notably, the non-swelling of glassy PS by IL allows the BCP to swell PMMA domains by large amounts, while preserving a mechanically rigid stretched PS honey-comb scaffold structure as discussed further below. Another neutralizing effect may come from the concentration gradient produced during evaporation of solvent. Preliminary AFM measurements on films cast from varying ratios of toluene and THF in the casting solution have shown that the in-plane distribution of cylinders changes with change in the casting solution.

3.5. Polystyrene as the structural support for swollen morphologies

Our results for SEA-IL of low M_n BCPs both with symmetric and asymmetric block volume fractions show an early transition in morphology at lower IL contents compared to high M_n BCPs caused due to alteration of the block volume fractions. Also, the IL contents for BCP films are much higher than that for stable homopolymer PMMA films blended with IL (show macrophase separation of IL at 30 mass% IL content). This suggests that PS does not uptake the IL and stays glassy which plays a major role as the structural component in stabilizing order at very high IL concentrations and that chain entanglements are important for morphology transitions. The *asym* PS-b-PMMA (M_n = 55 k-b-22 k) can hold up to 150 mass% IL before macrophase separation compared to only 50 mass% for low M_n (35 k-b-12.5 k) BCP. The higher molecular mass of PS (55 k compared to 35 k) in the former leads to a higher degree of chain entanglement in the matrix PS and stabilizes the IL-filled PMMA domains. When the pressure on the cylindrical walls from the segregated IL exceeds the counter pressure of entangled chains in the PS walls, domains start merging eventually causing a spillover producing bigger IL domains. The same applies to the *sym* BCP (M_n = 33 k-b-33 k) where the structural PS block is of a lower molecular mass and we observe domain merging and macrophase separation at lower IL contents compared to PS-b-PMMA (55 k-b-22 k) films. In essence, the spillover to form pure IL domains occurs early in the IL concentration range when the structural PS chains are absent or have poor entanglements at lower molecular mass.

3.6. BCP-IL based ultrafiltration membrane fabrication and performance

The significance of the structural support of the PS matrix becomes clearer from our etching experiments to remove the PMMA-IL domains for membrane fabrication. Selectively removing one block from the vertical microstructure will produce pores for applications like ultrafiltration membranes. While cylindrical microstructures will produce circular pores on the film surface, perpendicular lamellar microdomains will produce slits. For PS-b-PMMA, a UV vacuum treatment can be used to simultaneously crosslink the PS matrix and degrade and detach PMMA from the BCP. The etched PMMA is removed by immersion in a glacial acetic acid bath that also removes the IL leaving behind a crosslinked PS template. The PS crosslinking is very important for the vertical lamellar structures where we are left with free-standing PS walls after PMMA removal. We have used this methodology to fabricate nanoporous thin film membranes supported by commercial microporous polyether sulfone support membranes (PES). Thin films (50 nm–100 nm) are floated off on the surface of water from a PSS underlayer, received on the PES support, and etched via the method described in Fig. S14 to produce a membrane with isotropic nanoporous active BCP layer using cylinder forming BCPs and slit-shaped nanopores using lamellar BCPs. The IL content in the film can be increased to increase the cylinder diameter and consequently increase the pore size. Membranes with a PES support (average pore size 0.2 μm) and active BCP layer of PS-b-PMMA (55 k-b-22 k) with 30 mass%, 50 mass%, and 70 mass% IL were fabricated and tested for their transport and separation properties.

A dead-end pressure cell setup (Fig. S15) was used to perform DI water flux measurements and polymer filtration (dye-labeled Dextran in water) at 7.5 psi pressure (≈50 kPa). UV–visible spectroscopy was performed on the stock solutions and membrane permeates to quantify the separation efficiency/molecular weight cutoff. A representative dataset for a membrane with PS-b-PMMA (55 k-b-22 k) + 70 mass% IL active layer and tested for filtration of dextran (M_n = 500 kg/mol) is shown in Fig. 8(a). The reduction in absorbance intensity from dextran (at 400–500 nm wavelength) in the permeate shows excellent solute rejection.

Average results are shown in Fig. 8(b) where the films with higher IL content show improved flux due to bigger pore sizes. The average flux for a 70 mass% IL based BCP membrane is ≈ 240 L/h m^2 bar. The variability in flux increases with IL content due to increased dispersity in the shape and size of the pores. T. Ahmad et al. surveyed the performance of multiple polymer-based filtration membranes [48]. From their report, the average fluxes of most membranes were below 200 L/m^2 h bar with only a few candidates with flux over 300 L/m^2 h bar. Ahn et al. used PS-b-PMMA films thermally ordered on neutralized substrates as active membrane surfaces [6]. They achieved excellent BCP assembly and fluxes of about 128 L/m^2h at 1 bar pressure [6]. Hahn et al. developed PS-b-P4VP based membranes by SNIPS (solvent non-solvent induced phase separation) supported by PVDF (polyvinylidene fluoride) membranes [49]. They measured pH responsive fluxes and found a flux of about 400 L/m^2h bar for membranes with pore sizes of about 16 nm [49]. Membranes made from blending of different BCPs have also found attention and Yu et al. showed membranes made by using blends of PS-b-P4VP and poly(styrene-*b*-acrylic acid) (PS-*b*-PAA) [42]. The blending ratios allowed control over pore density and pure water fluxes as high as 592 L/m^2h were obtained at 1.37 bar pressure. Yu et al. also produced PS-b-P4VP membranes based on a micellar structure where they tuned the pore size by electroless gold deposition [42]. Increasing the amount of gold reduced the pore sizes reducing the water flux with best fluxes of 3000 L/m^2h bar obtained at 0.01 % gold addition [42]. For our BCP based films, the structural PS matrix becomes thinner with increasing IL concentration and may further cause flux variations due to pore shrinkage or expansion. The separation performance is presented in Fig. 8(c) and the separation cut-off size for a 90 % polymer rejection was found at ≈ 44 nm hydrodynamic diameter for 30 mass% and ≈62 nm hydrodynamic diameter for 70 mass% IL membranes for separating dye-labeled dextran from water. These cut-off sizes are higher than the cylinder diameters measured from as-cast film surface AFM images with the same IL content (37.6 ± 2.9 nm for 30 mass% IL and 54 ± 8.3 nm for 70 mass% IL). The pore sizes for membranes on PES supports were also measured using AFM (not accurate because the soft PES support distorts the measurements) and are 17.73 ± 2.8 nm for 30 mass% IL and 29.1 ± 5.4 nm for 70 mass% IL. There are a few reasons for the discrepancy between AFM measurements on Si wafers vs. those on flexible PES vs. the experimental cut-off polymer sizes.

Firstly, the cylindrical domains are highly swollen with IL in the as-cast state and are stabilized by the structural PS matrix. On the removal of IL after the etching process, the stress on the cylindrical walls is

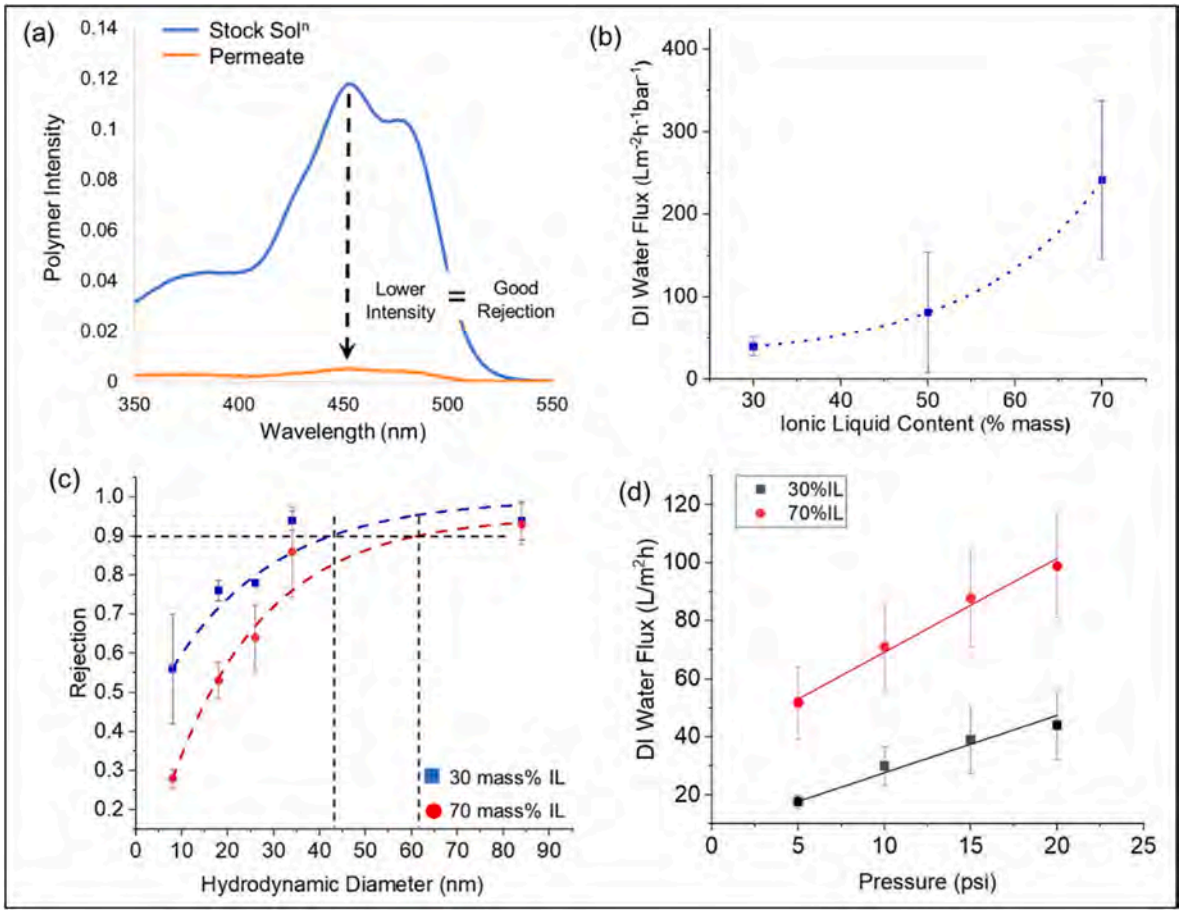

Fig. 8. Membrane performance for PS-b-PMMA (55 k-b-22 k) based membranes supported on a commercial PES membrane (average pore size of 0.2 μm) at 7.5 psi; (a) UV-viz spectra for Dye labeled Dextran (M_n = 500 kg/mol; 0.125 mg/ml in DI water) before (Stock) and after (Permeate) filtration test, (b) DI water fluxes for M_n = 55k-b-22k with 30 mass%, 50 mass% and 70 mass% IL, (c) Dextran rejection ratios for membranes from 30 mass% and 70 mass% IL loaded films crosslinked by 20 min UV in vacuum, (d) DI water flux for 30 mass% IL and 70 mass% IL based membrane vs. pressure showing a linear trend. Approx. hydrodynamic diameters (nm) and (molecular mass) for dextran are 8 (20 kg/mol), 18 (70 kg/mol), 26 (250 kg/mol), 34 (500 kg/mol), 84 (2000 kg/mol).

released and the pores shrink as in the AFM image of a membrane on PES. Secondly, the cut-off sizes are larger because the filtrations occur under pressure causing an expansion of the pores. Also, due to a limited set of Dextran molecular masses used, the actual cut-off size may be intermediate between the sizes that pass through the membrane and the measured cut-off sizes. The expansion of pores is also observed during flux tests at higher pressures where the normalized average flux increases for these membranes due to the expansion of pores and clearing of any blocked pores [50]. The enhancement in flux with pressure is measured and is presented in Fig. 8(d) for PS-b-PMMA (55 k-b-22 k) based membranes with 30 mass% and 70 mass% IL concentrations. The flux was observed to rapidly increase linearly with pressure with a slope of ≈3.2 L/m^{2}h psi and ≈2 L/m^{2}h psi for 70 mass% and 30 mass% membranes. The reusability of membranes is also an important parameter to optimize for commercialization. Al-Maas et al. tested the performance of supported PS-b-PMMA thin film membranes for oil-water separation and found that the membranes were stable to caustic (NaOH) cleaning [50]. In addition to polymeric separations, the pore sizes of these membranes are in the range of many biomolecules and can be used for their enrichment. Our preliminary results suggest that globular biomolecules like the high-value antibody IgG (Immunoglobin G) can be removed from its solution in phosphate-buffered saline using a PS-b-PMMA (55 k-b-22 k) with 30 mass% IL membrane. The antibody does not associate with the membrane, and we observed an average recovery of about 91 %. These observations point towards more room for the optimization of the etching treatment for better matrix stability and fully etched pores. Some of our experiments do show enhanced fluxes for membranes treated for extended time in the UV-vacuum chamber likely due to better PS crosslinking and PMMA etching.

Besides particulate or polymer filtration, these membranes show great prospects in oil/water filtration applications. Zeta potential measurements performed for etched membranes show positive values of approximately 35 mV–40 mV indicating the presence of a positive charge on the membranes. These charges are due to the scission of the PMMA chains from PS at the pore boundaries. This makes them excellent candidates for wettability-based separations like oil/water for wastewater management. Preliminary separation tests performed using mixtures of DI water and dye-labeled heptane (red) as the oil substitute show good potential for oil/water filtration. Fig. S16 shows a set of the heptane/water mixtures used for the filtration test and resulting permeate and retentate solutions where the permeate is clear water due to its higher affinity towards the charged pores, allowing it to flow through. Because these are wettability-based separations, high molecular mass BCPs that develop bigger pores and have higher fluxes can be used to perform oil/water separation. A membrane made from PS-b-PMMA (235 k-b-263 k) with 50 mass% IL (structure shown in Fig. S12) on a 0.2 μm PES support has an average normalized flux of (441 ± 256 Lm^{-2}h^{-1}bar^{-1}). These fluxes are higher or very close to some of the examples discussed earlier. The flux variability may be due to pore shrinkage under pressure which is significant for larger pores. Optimizing the fabrication method (increasing crosslinking) may resolve these issues. When a low molecular mass symmetric BCP is used to develop a slit-like membrane structure, shape-selective separations can be performed. Separating globular molecules that get blocked vs. rod or helical molecules like the tobacco mosaic virus that can pass through the slits becomes possible. Another potential application for these membranes can be found in ionic separations. Due to the presence of IL in the PMMA channels running through the thickness of an unetched membrane, the PMMA chains are highly mobile. This structure can be used to separate or conduct ions based on size as well as affinity with the IL and similar BCP structures have been studied for ion conduction applications [51–53]. Optimizing the SEA-IL method for low M_n symmetric BCPs that produce vertical slits will make the technique applicable for lithography processes where a BCP layer can be used to rectify defects in the EUV photolithography patterns [11,12,54–56].

4. Conclusions

Both the AFM and GISAXS characterization indicate that beyond a specific IL concentration, the reduction in the glass transition temperature and neutralization of substrate interactions are significantly strong, and the evaporation rate of the toluene-THF solvent mixture is effective in inducing vertical order in as-cast films. Thinner films were observed to have better vertical order despite the greater enthalpic influence of the substrate. On the contrary, due to this substrate influence, thinner films have parallel domain orientations when processed thermally. We speculate that for SEA-IL-ordered thin films, faster solidification of the film on solvent evaporation favors lower tortuosity of vertical domains. As the film thickness increases, the solvent evaporation front gives more time for the film to solidify and the microstructure to develop. This in turn allows the enthalpic interactions to make the IL-filled cylinders more tortuous and is observed in the GISAXS analysis for thick films. The vertical orientation further improved with an increase in the IL content and can be attributed to better film plasticization and neutralization of interfacial interactions. There is more work to be done to understand the evolution of the vertical microstructure and the effects of different substrates and IL-BCP combinations. In-situ GISAXS experiments will allow us to gain insight into the microstructure development as the solvent evaporates. RSoXS measurements can reveal the distribution of IL in the swollen PMMA domains. The effect of the Flory Huggins parameter can be explored by extending the one-step SEA method to high χ BCPs. A library of IL-BCP pairs can be generated using high throughput artificial intelligence machine learning-based screening techniques to screen out potential candidates with microstructures useful in nanolithography and isoporous ultra and nanofiltration membranes. Optimization of the membrane fabrication method can lead to better membrane performance.

Disclaimer

Certain commercial materials, software and equipment are identified to specify adequately the experimental procedure. In no case does such identification imply a recommendation by the National Institute of Standards and Technology, nor does it imply that the material or equipment identified is necessarily the best available for this purpose.

Funding

We acknowledge NSF DMR 1905996 and Welch grants E-2105-20220331 and V-E-0001-20230731 for support of the research.

Supporting information available

Includes AFM images, Optical images, and GISAXS profiles for analysis made on as-cast PMMA, PS-b-PMMA, PS-b-P4VP, and PS-b-PEO films.

CRediT authorship contribution statement

Kshitij Sharma: Writing – review & editing, Writing – original draft, Methodology, Investigation, Formal analysis, Data curation, Conceptualization. **Khadar Basha Shaik:** Writing – review & editing, Investigation. **Maninderjeet Singh:** Formal analysis, Writing – review & editing. **Tanguy Terlier:** Investigation. **Aidan Coffey:** Investigation. **Chenhui Zhu:** Writing – review & editing, Investigation. **Joseph Strzalka:** Writing – review & editing, Investigation. **Alamgir Karim:** Writing – review & editing, Funding acquisition, Conceptualization.

Declaration of competing interest

The authors declare the following financial interests/personal relationships which may be considered as potential competing interests:

Alamgir Karim reports financial support was provided by National Science Foundation. If there are other authors, they declare that they have no known competing financial interests or personal relationships that could have appeared to influence the work reported in this paper.

Data availability

Data will be made available on request.

Acknowledgments

We would like to acknowledge support from Dr. Devin L. Shaffer at the Department of Civil & Environmental Engineering, University of Houston for UV–vis spectroscopy and zeta potential measurements. We acknowledge the support from Dr. Richard C. Wilson and his student Vijay Maranholkar at the Department of Chemical & Biomolecular Engineering, University of Houston for the materials and measurements on IgG separation. This research used beamline 7.3.3 of the Advanced Light Source, which is a DOE Office of Science User Facility under contract no. DE-AC02-05CH11231. This research used resources of the Advanced Photon Source, a U.S. Department of Energy (DOE) Office of Science user facility operated for the DOE Office of Science by Argonne National Laboratory under Contract No. DE-AC02-06CH11357. We also acknowledge the user facilities at the University of Houston nanofabrication facility and at Columbia University for SEM imaging.

Appendix A. Supplementary data

Supplementary data to this article can be found online at https://doi.org/10.1016/j.memsci.2024.123102.

References

[1] R.A. Segalman, Patterning with block copolymer thin films, Mater. Sci. Eng. R Rep. (February 28, 2005) 191–226, https://doi.org/10.1016/j.mser.2004.12.003.
[2] C. Park, J. Yoon, E.L. Thomas, Enabling Nanotechnology with self assembled block copolymer patterns, Polymer 3 (2003) 6725–6760, https://doi.org/10.1016/j.polymer.2003.08.011. Elsevier BV October.
[3] S.P. Nunes, Block copolymer membranes, in: Sustainable Nanoscale Engineering: from Materials Design to Chemical Processing, Elsevier, 2019, pp. 297–316, https://doi.org/10.1016/B978-0-12-814681-1.00011-4.
[4] N. Hampu, J.R. Werber, W.Y. Chan, E.C. Feinberg, M.A. Hillmyer, Next-generation ultrafiltration membranes enabled by block polymers, ACS Nano. Am. Chem. Soc. December 22 (2020) 16446–16471, https://doi.org/10.1021/acsnano.0c07883.
[5] Y. Luo, X. Wang, R. Zhang, M. Singh, A. Ammar, D. Cousins, M.K. Hassan, D. Ponnamma, S. Adham, M.A.A. Al-Maadeed, A. Karim, Vertically oriented nanoporous block copolymer membranes for oil/water separation and filtration, Soft Matter 16 (42) (2020) 9648–9654, https://doi.org/10.1039/d0sm00526f.
[6] H. Ahn, S. Park, S.W. Kim, P.J. Yoo, D.Y. Ryu, T.P. Russell, Nanoporous block copolymer membranes for ultrafiltration: a simple approach to size tunability, ACS Nano 8 (11) (2014) 11745–11752, https://doi.org/10.1021/nn505234v.
[7] S. Takamuku, P. Jannasch, Multiblock copolymers containing highly sulfonated poly(Arylene sulfone) blocks for Proton conducting electrolyte membranes, Macromolecules 45 (16) (2012) 6538–6546, https://doi.org/10.1021/ma301245u.
[8] L. Lei, Y. Xia, X. Chen, S. Shi, Long-range-ordered, hexagonally packed nanoporous membranes from Degradable-block-containing diblock copolymer film templates, J. Appl. Polym. Sci. 5 (2014), https://doi.org/10.1002/app.39638. January.
[9] M. Singh, A. Agrawal, W. Wu, A. Masud, E. Armijo, D. Gonzalez, S. Zhou, T. Terlier, C. Zhu, J. Strzalka, K. Matyjaszewski, M. Bockstaller, J.F. Douglas, A. Karim, Soft-shear-aligned vertically oriented lamellar block copolymers for template-free sub-10 Nm patterning and Hybrid Nanostructures, ACS Appl. Mater. Interfaces 14 (10) (2022) 12824–12835, https://doi.org/10.1021/acsami.1c23865.
[10] F.S. Bates, G.H. Fredrickson, Block copolymers-Designer soft materials, Phys. Today 52 (2) (1999) 32–38, https://doi.org/10.1063/1.882522.
[11] R. Ruiz, H. Kang, F.A. Detcheverry, E. Dobisz, D.S. Kercher, T.R. Albrecht, J.J. De Pablo, P.F. Nealey, Density Multiplication and improved lithography by directed block copolymer assembly, Science 321 (5891) (2008) 936–939, https://doi.org/10.1126/science.1157626, 1979.
[12] C.M. Bates, M.J. Maher, D.W. Janes, C.J. Ellison, C.G. Willson, Block copolymer lithography, Macromolecules 14 (2014) 2–12, https://doi.org/10.1021/ma401762n. January.
[13] G. Coulon, T.P. Russell, V.R. Deline, P.F. Green, Surface-induced orientation of symmetric, diblock copolymers: a secondary ion mass Spectrometry study, Macromolecules 22 (6) (1989) 2581–2589, https://doi.org/10.1021/ma00196a006.
[14] J. Bang, J. Bae, P. Lówenhielm, C. Spiessberger, S.A. Given-Beck, T.P. Russell, C. J. Hawker, Facile Routes to patterned surface neutralization layers for block copolymer lithography, Adv. Mater. 19 (24) (2007) 4552–4557, https://doi.org/10.1002/adma.200701866.
[15] E.J.W. Crossland, S. Ludwigs, M.A. Hillmyer, U. Steiner, Freestanding Nanowire Arrays from soft-etch block copolymer templates, Soft Matter 3 (1) (2007) 94–98, https://doi.org/10.1039/b609780d.
[16] H. Hu, M. Gopinadhan, C.O. Osuji, Directed self-assembly of block copolymers: a Tutorial review of Strategies for enabling Nanotechnology with soft Matter, Soft Matter. Royal Soc. Chem. June 14 (2014) 3867–3889, https://doi.org/10.1039/c3sm52607k.
[17] G. Singh, S. Batra, R. Zhang, H. Yuan, K.G. Yager, M. Cakmak, B. Berry, A. Karim, Large-scale Roll-to-Roll fabrication of vertically oriented block copolymer thin films, ACS Nano 7 (6) (2013) 5291–5299, https://doi.org/10.1021/nn401094s.
[18] A. Böker, H. Elbs, H. Hänsel, A. Knoll, S. Ludwigs, H. Zettl, V. Urban, V. Abetz, A. H. Müller, G. Krausch, Microscopic mechanisms of electric-field-induced alignment of block copolymer microdomains, Phys. Rev. Lett. 89 (13) (2002) 1355021–1355024, https://doi.org/10.1103/physrevlett.89.135502.
[19] B.C. Berry, A.W. Bosse, J.F. Douglas, R.L. Jones, A. Karim, Orientational order in block copolymer films zone annealed below the order-Disorder transition temperature, Nano Lett. 7 (9) (2007) 2789–2794, https://doi.org/10.1021/nl071354s.
[20] S. Samant, S.T. Hailu, A.M. Al-Enizi, A. Karim, D. Raghavan, Orientation control in Nanoparticle filled block copolymer cold zone annealed films, J. Polym. Sci. B Polym. Phys. 53 (8) (2015) 604–614, https://doi.org/10.1002/polb.23684.
[21] P. Mansky, Y. Liu, E. Huang, T.P. Russell, C. Hawker, Controlling polymer-surface interactions with random copolymer Brushes, Science (275) (1997) 1458–1460, 1979.
[22] A. Modi, S.M. Bhaway, B.D. Vogt, J.F. Douglas, A. Al-Enizi, A. Elzatahry, A. Sharma, A. Karim, Direct immersion annealing of thin block copolymer films, ACS Appl. Mater. Interfaces 7 (39) (2015) 21639–21645, https://doi.org/10.1021/acsami.5b06259.
[23] M. Longanecker, A. Modi, A. Dobrynin, S. Kim, G. Yuan, R. Jones, S. Satija, J. Bang, A. Karim, Reduced domain size and interfacial Width in Fast ordering Nanofilled block copolymer films by direct immersion annealing, Macromolecules 49 (22) (2016) 8563–8571, https://doi.org/10.1021/acs.macromol.6b01690.
[24] K. Sharma, A. Agrawal, A. Masud, S.K. Satija, J.F. Ankner, J.F. Douglas, A. Karim, Hiking down the free energy Landscape using sequential solvent and thermal processing for versatile ordering of block copolymer films, ACS Appl. Mater. Interfaces 15 (17) (2023) 21562–21574, https://doi.org/10.1021/acsami.2c21924.
[25] W.I. Park, J.M. Kim, J.W. Jeong, Y.S. Jung, Deep-nanoscale pattern Engineering by immersion-induced self-assembly, ACS Nano 8 (10) (2014) 10009–10018, https://doi.org/10.1021/nn504995c.
[26] K. Sharma, M. Singh, S.K. Satija, J.F. Ankner, J.F. Douglas, A. Karim, Transient interfacial pattern formation in block copolymer thin films via sequential thermal and solvent immersion annealing, ACS Appl. Mater. Interfaces 16 (2024) 15569–15585, https://doi.org/10.1021/acsami.4c00068.
[27] A. Masud, W. Wu, M. Singh, W. Tonny, A. Ammar, K. Sharma, J.W. Strzalka, T. Terlier, J.F. Douglas, A. Karim, Solvent processing and ionic liquid-Enabled long-range vertical ordering in block copolymer films with enhanced film stability, Macromolecules 54 (18) (2021) 8512–8525, https://doi.org/10.1021/acs.macromol.1c01305.
[28] G. Kim, M. Libera, Morphological development in solvent-cast Polystyrene-Polybutadiene-Polystyrene (SBS) triblock copolymer thin films, Macromolecules 31 (8) (1998) 2569–2577. https://pubs.acs.org/sharingguidelines.
[29] S.H. Kim, M.J. Misner, T. Xu, M. Kimura, T.P. Russell, Highly oriented and ordered Arrays from block copolymers via solvent evaporation, Adv. Mater. 16 (3) (2004) 226–231, https://doi.org/10.1002/adma.200304906.
[30] R.M. Ho, W.H. Tseng, H.W. Fan, Y.W. Chiang, C.C. Lin, B.T. Ko, B.H. Huang, Solvent-induced microdomain orientation in Polystyrene-b-poly(l-Lactide) diblock copolymer thin films for Nanopatterning, Polymer (Guildf) 46 (22) (2005) 9362–9377, https://doi.org/10.1016/j.polymer.2005.07.069.
[31] S. Park, J.Y. Wang, B. Kim, W. Chen, T.P. Russell, Solvent-induced transition from micelles in solution to cylindrical microdomains in diblock copolymer thin films, Macromolecules 40 (25) (2007) 9059–9063, https://doi.org/10.1021/ma071321z.
[32] T.M. Bennett, K. Pei, H.-H. Cheng, K.J. Thurecht, K.S. Jack, I. Blakey, Can ionic liquid additives Be used to extend the Scope of poly(styrene)-block-poly(methyl methacrylate) for directed self-assembly? J. Nanolithogr. MEMS, MOEMS 13 (3) (2014) 031304 https://doi.org/10.1117/1.jmm.13.3.031304.
[33] X. Chen, C. Zhou, S.J. Chen, G.S.W. Craig, P. Rincon-Delgadillo, T. Dazai, K. Miyagi, T. Maehashi, A. Yamazaki, R. Gronheid, M.P. Stoykovich, P.F. Nealey, Ionic liquids as additives to Polystyrene- block-poly(methyl methacrylate) enabling directed self-assembly of patterns with sub-10 Nm features, ACS Appl. Mater. Interfaces 10 (19) (2018) 16747–16759, https://doi.org/10.1021/acsami.8b02990.
[34] A. Masud, M. Longanecker, S. Bhadauriya, M. Singh, W. Wu, K. Sharma, T. Terlier, A.M. Al-Enizi, S. Satija, J.F. Douglas, A. Karim, Ionic liquid enhanced parallel lamellar ordering in block copolymer films, Macromolecules 54 (10) (2021) 4531–4545, https://doi.org/10.1021/acs.macromol.0c02546.
[35] B.B. Sauer, R.S. Mclean, R.R. Thomas, Tapping mode AFM studies of Nano-phases on Fluorine-containing Polyester coatings and Octadecyltrichlorosilane Monolayers, Langmuir 14 (1998) 3045–3051.
[36] Y. He, Y. Yan, Y. Geng, Morphology measurements by AFM tapping without causing surface damage: a phase Shift characterization, Ultramicroscopy 254 (2023), https://doi.org/10.1016/j.ultramic.2023.113832.

[37] D. Wang, X. Bin Liang, Y.H. Liu, S. Fujinami, T. Nishi, K. Nakajima, Characterization of surface Viscoelasticity and energy Dissipation in a polymer film by atomic force microscopy, Macromolecules 44 (21) (2011) 8693–8697, https://doi.org/10.1021/ma201148f.
[38] T.M. Bennett, K.S. Jack, K.J. Thurecht, I. Blakey, Perturbation of the experimental phase Diagram of a diblock copolymer by blending with an ionic liquid, Macromolecules 49 (1) (2016) 205–214, https://doi.org/10.1021/acs.macromol.5b02041.
[39] M. Radjabian, V. Abetz, Advanced porous polymer membranes from self-Assembling block copolymers. Progress in Polymer Science, Elsevier Ltd, March 1, 2020, https://doi.org/10.1016/j.progpolymsci.2020.101219.
[40] M. Radjabian, C. Abetz, B. Fischer, A. Meyer, V. Abetz, Influence of solvent on the structure of an Amphiphilic block copolymer in solution and in formation of an Integral asymmetric membrane, ACS Appl. Mater. Interfaces 9 (37) (2017) 31224–31234, https://doi.org/10.1021/acsami.6b15199.
[41] X. Qiu, H. Yu, M. Karunakaran, N. Pradeep, S.P. Nunes, K.V. Peinemann, Selective separation of similarly sized Proteins with tunable nanoporous block copolymer membranes, ACS Nano 7 (1) (2013) 768–776, https://doi.org/10.1021/nn305073e.
[42] H. Yu, X. Qiu, S.P. Nunes, K.V. Peinemann, Self-assembled isoporous block copolymer membranes with tuned pore sizes, Angew. Chem. Int. Ed. 53 (38) (2014) 10072–10076, https://doi.org/10.1002/anie.201404491.
[43] L. Li, Y. Zhong, J. Li, C. Chen, A. Zhang, J. Xu, Z. Ma, Thermally stable and solvent Resistant Honeycomb structured Polystyrene films via Photochemical cross-Linking, J. Mater. Chem. 19 (39) (2009) 7222–7227, https://doi.org/10.1039/b911714h.
[44] D.M. Wiles, D.J. Carlsson, PHOTOSTABILISATI ON MECHANISMS IN polymers: a REVIEW*5, Polym. Degrad. Stabil. 3 (1980) 61–72.
[45] M.J. Fasolka, P. Banerjee, A.M. Mayes, G. Pickett, A.C. Balazs, Morphology of ultrathin supported diblock copolymer films: Theory and experiment, Macromolecules 33 (15) (2000) 5702–5712, https://doi.org/10.1021/ma990021h.
[46] H.S. Suh, H. Kang, P.F. Nealey, K. Char, Thickness dependence of neutral parameter windows for perpendicularly oriented block copolymer thin films, Macromolecules 43 (10) (2010) 4744–4751, https://doi.org/10.1021/ma100150j.
[47] J.H. Gibbs, E.A. DiMarzio, Nature of the glass transition and the glassy state, J. Chem. Phys. 28 (3) (1958) 373–383, https://doi.org/10.1063/1.1744141.
[48] T. Ahmad, C. Guria, A. Mandal, A review of oily wastewater treatment using ultrafiltration membrane: a Parametric study to enhance the membrane performance, J. Water Proc. Eng. 1 (2020), https://doi.org/10.1016/j.jwpe.2020.101289. Elsevier Ltd August.
[49] J. Hahn, J.I. Clodt, C. Abetz, V. Filiz, V. Abetz, Thin isoporous block copolymer membranes: it is all about the process, ACS Appl. Mater. Interfaces 7 (38) (2015) 21130–21137, https://doi.org/10.1021/acsami.5b04658.
[50] M. Al-Maas, A. Hussain, J. Minier-Matar, M.K. Hassan, M.A.A. Al-Maadeed, K. Alamgir, S. Adham, Performance Evaluation of Emerging block copolymer membranes for oil-water separation, Green Technol., Resilience, Sustain. 2 (1) (2022), https://doi.org/10.1007/s44173-022-00004-0.
[51] M.L. Hoarfrost, R.A. Segalman, Ionic Conductivity of Nanostructured block copolymer/ionic liquid membranes, Macromolecules 44 (13) (2011) 5281–5288, https://doi.org/10.1021/ma200060g.
[52] C.G. Arges, Y. Kambe, H.S. Suh, L.E. Ocola, P.F. Nealey, Perpendicularly aligned, anion conducting Nanochannels in block copolymer electrolyte films, Chem. Mater. 28 (5) (2016) 1377–1389, https://doi.org/10.1021/acs.chemmater.5b04452.
[53] C.G. Arges, Y. Kambe, M. Dolejsi, G.P. Wu, T. Segal-Pertz, J. Ren, C. Cao, G.S. W. Craig, P.F. Nealey, Interconnected ionic domains enhance Conductivity in microphase separated block copolymer electrolytes, J. Mater. Chem. A Mater. 5 (11) (2017) 5619–5629, https://doi.org/10.1039/c6ta10838e.
[54] S. Xiong, L. Wan, Y. Ishida, Y.A. Chapuis, G.S.W. Craig, R. Ruiz, P.F. Nealey, Directed self-assembly of triblock copolymer on chemical patterns for sub-10-nm nanofabrication via solvent annealing, ACS Nano 10 (8) (2016) 7855–7865, https://doi.org/10.1021/acsnano.6b03667.
[55] G.S. Doerk, J.Y. Cheng, G. Singh, C.T. Rettner, J.W. Pitera, S. Balakrishnan, N. Arellano, D.P. Sanders, Enabling complex Nanoscale pattern Customization using directed self-assembly, Nat. Commun. 5 (2014), https://doi.org/10.1038/ncomms6805.
[56] J. Cheng, G.S. Doerk, C.T. Rettner, G. Singh, M. Tjio, H. Truong, N. Arellano, S. Balakrishnan, M. Brink, H. Tsai, C.-C. Liu, M. Guillorn, D.P. Sanders, Customization and Design of directed self-assembly using Hybrid Prepatterns, in: Alternative Lithographic Technologies, vol. 9423, VII, SPIE, 2015 942307, https://doi.org/10.1117/12.2086973.